Chapter 3

Experiment Specifications and Event Spectra

In section 3.1, we give an overview of T2K-II, NOνA-II and JUNO: the terrestrial neutrino oscillation experiments considered in this thesis. In section 3.2, we introduce the simulation software GLoBES used in our statistical analysis of the experiments. We discuss the simulation technique adopted to study the physics potential of the experiments. We describe the experiments using updated information on fluxes, signal and background efficiencies, and systematic errors. We present criteria for the signal and background event selection procedures. Finally, in section 3.3, we present our results on the event spectra for the selected ν_e ($\bar{\nu}_e$) appearance and ν_μ ($\bar{\nu}_\mu$) disappearance channels for A-LBL experiments T2K-II and NOνA-II, as well as $\bar{\nu}_e$ disappearance channel of R-MBL experiment JUNO.

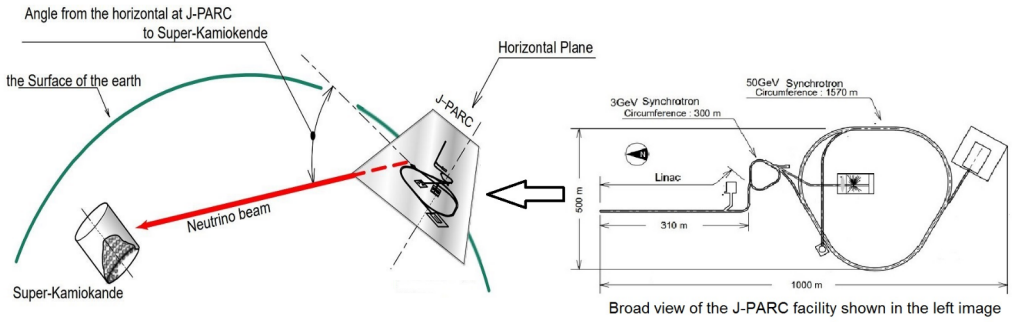

Figure 3-1: A Schematic diagram of J-PARC, Tokai to Super-K detector, Kamioka. Images taken from Mishima K, et al. 9th International Workshop on Accelerator Alignment, September 26-29, 2006.

3.1 Specifications of the Terrestrial Neutrino Oscillation Experiments

3.1.1 T2K-II

Tokai-To-Kamioka (T2K) [1] is the second generation of accelerator-based long-baseline (A-LBL) neutrino oscillation experiments located in Japan. T2K-II [2] is a proposal to extend the T2K run until 2026 before Hyper-Kamiokande (HK) [3] starts operation. At the Japan Proton Accelerator Research Centre (J-PARC), protons of 3 GeV energy are accelerated to 30 GeV to produce a powerful beam intensity of about 0.77 MW. Pions and kaons are produced at the interaction of the 30 GeV proton beam from the (*See Figure* 3-1) Main Ring (MR) with a graphite target, 91.4 cm long and 2.6 cm in diameter, with a density of 1.8 g/cm^3. Pions are focused by three magnetic horns to increase the neutrino beam's intensity. A muon neutrino beam is produced from the decay products of pions and kaons. The properties of the neutrinos are measured at near detectors placed 280 m from the target, and the oscillation analysis is performed at the far detector, Super-Kamiokande (SK), which is located 295 km away.

The off-axis beam method is used to generate a narrow-band neutrino beam, as per Equations 1.12 and 1.13. The beam axis is slightly shifted away at an average angle of 2.5^o w.r.t the direction of the proton beam in order for SK to receive a neutrino beam with a peak energy of 0.6 GeV, close to the first oscillation maxima.

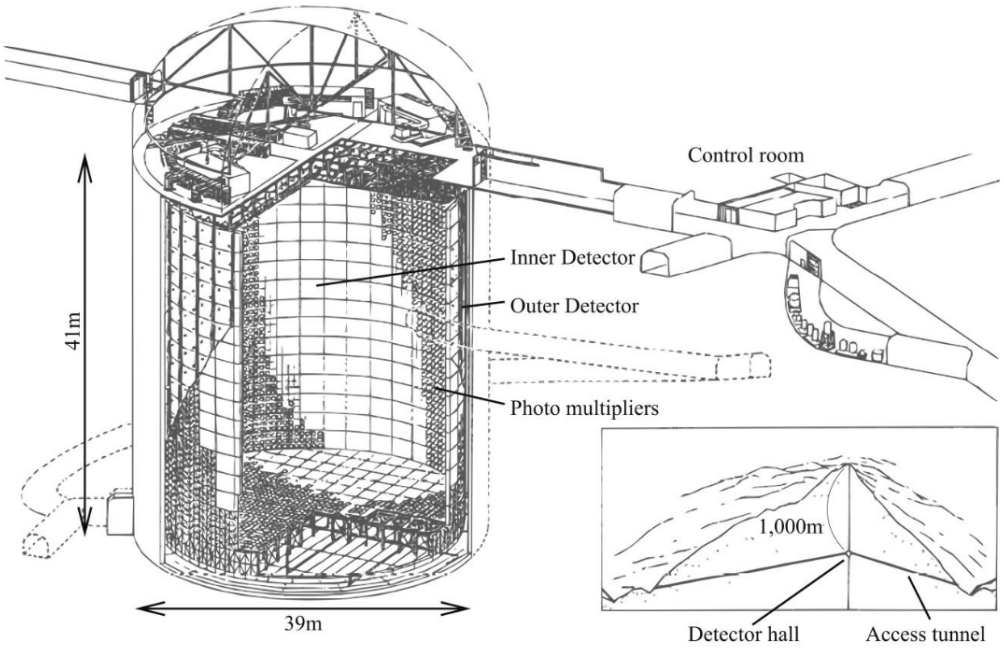

Figure 3-2: Schematic of T2K far neutrino detector: Super Kamiokande [8].

This technique increases the the fraction of CCQE events in energy range less than 1 GeV. For the event selection and energy reconstruction at SK, the CCQE events are signals while other CC events are background.

T2K Near and Far Detectors The T2K near neutrino detectors are composed of the neutrino beam monitor (INGRID) [4] and the neutrino spectrometer (ND280) [1, 5, 6]. These detectors are set in a pit inside the ND280 hall. The pit has a diameter of 17.5 m and a depth of 37 m. The ND280 detector measures the off-axis neutrino flux and energy spectrum at a baseline of 280 m. The off-axis angle to ND280 from the target position is 2.04°. This angle was chosen to make the neutrino spectrum at ND280 as similar as possible to the spectrum at SK. The neutrino beam intensity and direction are monitored directly by measuring the profile of neutrinos at the INGRID detector [7], located 280 m away from the target.

Super-Kamiokande is the far detector and an upgrade of the previous Kamiokande detector, and it measures the event rate and energy spectrum in the off-axis direction at a baseline of 295 km. The detector lies under the peak of Mt. Ikenoyama, with 1000 metres of rock overburden at geographical co-ordinates

36°25′32.6″N and 137°18′37.1″E. The water Cherenkov detector consists of a welded stainless steel tank of 39m diameter and 42m tall with nominal capacity of 50ktons supported by an array of 11,146 50cm-diameter hemispherical inward-facing and 1885 outward facing 20cm-diameter hemispherical PMTs [9]. Neutrinos are detected with the PMTs by measuring the Cherenkov lights emitted by charged particles from the neutrino interactions in the water. The particle's vertex, energies, and directions are reconstructed from the timing and position of the Cherenkov lights. The particle identification (muon/electron separation) is performed based on the edge of the Cherenkov lights: the Cherenkov lights produced by muons have a sharp outer ring edge, while the Cherenkov lights produced by electrons have characteristically fuzzy edges due to electromagnetic showers. More details of SK are described in [10, 11].

SK provides excellent performance in reconstructing the neutrino energy and the neutrino flavor classification. This capability allows T2K(-II) to measure simultaneously the disappearance of muon (anti-)neutrinos and the appearance of electron (anti-)neutrinos from the flux of almost pure muon (anti-)neutrinos. While the data samples of the ν_μ ($\overline{\nu}_\mu$) disappearance provide a precise measurement of the atmospheric neutrino parameters, $\sin^2 2\theta_{23}$ and Δm^2_{31}, the ν_e ($\bar{\nu}_e$) appearance rates are driven by $\sin^2 2\theta_{13}$ and sensitive to $\delta_{\rm CP}$ and MH. T2K made an observation of electron neutrinos appearing from a muon neutrino beam [12] and presented an indication of CPV in the neutrino oscillation [13]. T2K originally planned to take data equivalent to 7.8×10^{21} protons-on-target (POT) exposure. In Neutrino 2020 conference, T2K [14] reported a collected data sample from 3.6×10^{21} POT exposure. In Ref. [2], T2K proposes to extend the run until 2026 and collect 20×10^{21} POT, allowing T2K to explore CPV with a confidence level (C.L.) of 3σ or higher if $\delta_{\rm CP}$ is close to $-\pi/2$ and make precision measurements of θ_{23} and $|\Delta m^2_{31}|$.

3.1.2 NOνA-II

NuMI Off-axis ν_e Appearance (NOνA) [15] is also the 2nd generation of A-LBL neutrino experiments placed in the US with a baseline of 810 km between the production source and the far detector. NOνA, similar to T2K(-II), adopts the off-axis technique such that the far detector is placed at an angle of 14 mrad to the averaged direction of the neutrino beam, with the oscillation maxima at about 2 GeV. The experiment aims to answer the same questions, but with different sensitivities to different parameters, depending on the baseline and the range of beam energies [16].

3.1.2.1 The NuMI beam

The NuMI beam at Fermilab [17] is designed to produce neutrinos and antineutrinos at high intensity by colliding a proton beam onto a fixed target. The proton beam is first accelerated to 8 GeV in a rapid cycling synchrotron called the Booster and then delivered to the Main Injector ring. The Main Injector accelerates the protons to 120 GeV that hit the 1.2 m graphite target. Operating at around 742 kW, the Main Injector is able to deliver $\sim 6 \times 10^{20}$ POT every year. The schematic diagram of the proton accelerator is shown in Figure 1-6. The production of mesons is similar to that of T2K(-II), the decay of which produces the neutrinos and antineutrinos when the magnetic horns with a current of 200kA defocus the mesons into a 675m long decay pipe. The neutrino energy range for oscillation analysis is 1-5 GeV for the experiment.

3.1.2.2 NOνA detectors

NOνA uses a near detector [18], located 1 km away from the production target, to characterize the unoscillated neutrino flux. The NOνA far detector is filled with liquid scintillator contained in PVC cells, totally weighted up 14 ktons with 63% active materials. Both the ND and FD are functionally identical, differing primarily in their sizes with the ND being 290 tons. The schematic diagram of

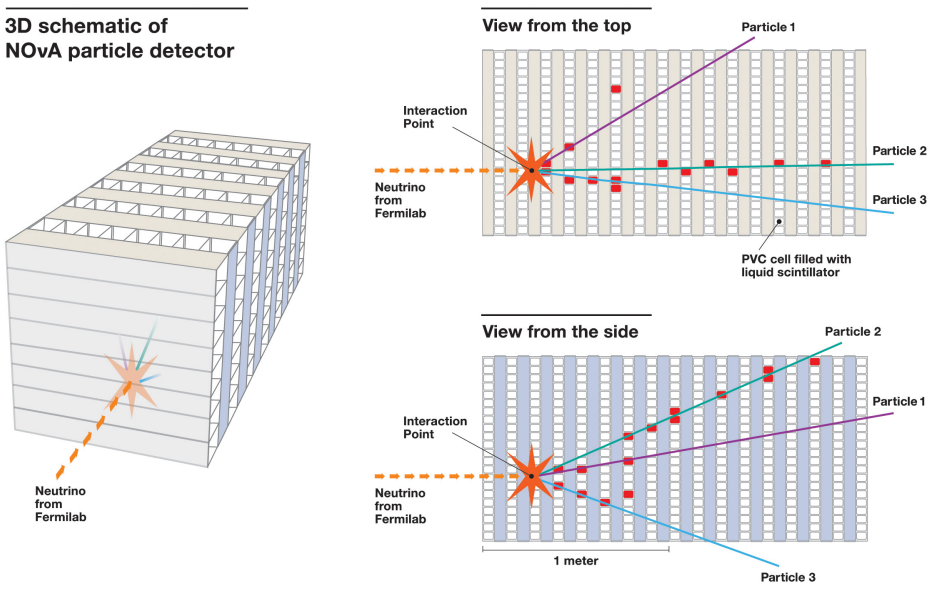

Figure 3-3: A graphic representation of one of the first neutrino interactions captured at the NOvA far detector in northern Minnesota. The dotted red line represents the neutrino beam, generated at Fermilab in Illinois and sent through 500 miles of earth to the far detector. The image on the left is a simplified 3-D view of the detector, the top right view shows the interaction from the top of the detector, and the bottom right view shows the interaction from the side of the detector. The information is reproduced from https://vms.fnal.gov/asset.

the NOνA detector is shown in Figure 3-3. The Far Detector has a dimension of $15.8m \times 15.8m \times 60m$, while the ND is of dimensions $3.8m \times 3.8m \times 15.9m$. The Far Detector is placed on surface in a detector hall with a modest overburden of 1.2 m concrete and 15 cm barite. It collects an enormous number of cosmic rays, the fundamental background to the oscillation analysis. The Near Detector is placed 100 m underground, where cosmic rays are negligible. NOνA takes advantage of machine learning for particle classification to enhance the event selection performance.

The event reconstruction of interactions in the detector deals with clustering calibrated hits, which characterize the topology of the interaction and thereby, identify the neutrino flavor and the incoming neutrino energy. The major interaction types that are relevant for the oscillation analysis are CCν_μ, CCν_e, NC and Cosmic muons. CCν_μ events are identifiable by a long and straight muon track made up of minimum ionizing hits. CCν_e evenets are characterized by an electron in the final state which produces a roughly conical shower cascade

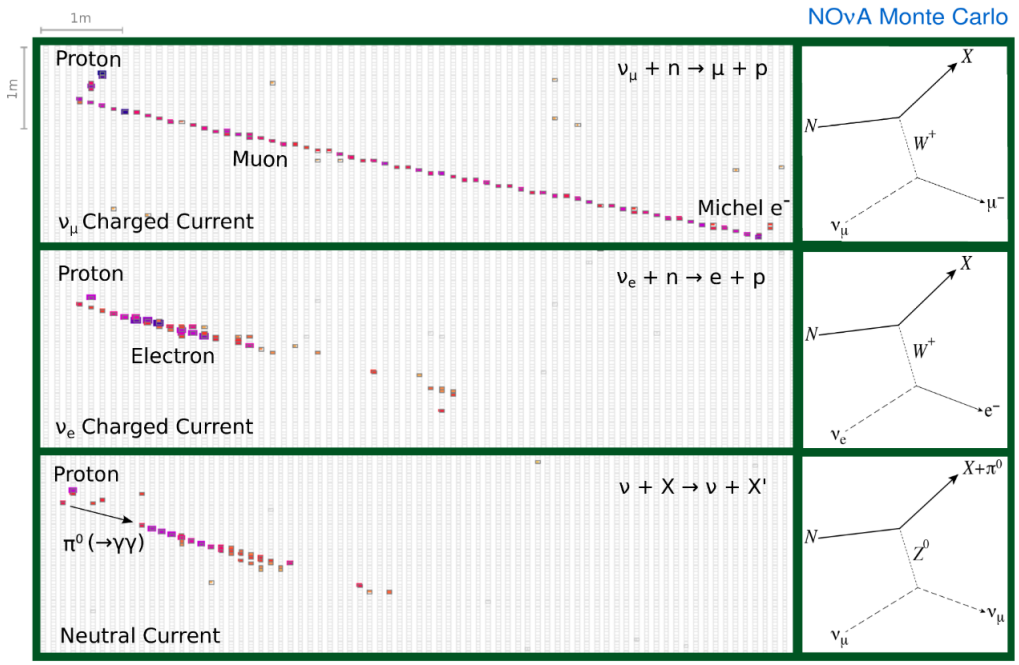

Figure 3-4: Interaction topologies for CCν_μ (*top*), CCν_e (*middle*) and NC (*bottom*) neutrino interactions [18] .

driven by pair production as the electron interacts with the dense material. It is difficult to separate oscillated CCν_e events and events coming from the intrinsic beam contamination. As a result, the beam CCν_e component is an irreducible background to the appearance channel. NC events are flavor independent interactions where the observed final state particles are only the hadronic component, as the neutrino just scatters off the nuclei and can't be observed. If the hadronic component involves a π^0, then, the decay can mimic CCν_e events at typical energies. Charged pions can also be produced resulting in track like topologies, which can be misidentified as short muon tracks and thus CCν_μ events. Hence, these events are important backgrounds to both oscillation channels. Charged Muons from cosmic ray interactions are also important backrounds. Most of them are long muon tracks coming in from the top of the detector and can be differentiated by their directions from a CCν_μ event. Some of them can also emit bremsstrahlung radiation at a variety of angles, which is sufficiently energetic to mimic CCν_e events. Examples of interaction topologies seen at the NOvA detectors for different types of neutrino interactions are shown in Figure 3-4.

In 2018 [19], NOνA provided more than 4σ C.L. evidence of electron anti-neutrino

appearance from a beam of muon anti-neutrinos. In Neutrino 2020 conference, NOνA [20] reported a collected data sample from 2.6×10^{21} POT exposure. In [21], NOνA offers the possibility of extending the run through 2024, hereby called NOνA-II, in order to get 3σ C.L. or higher sensitivity to the MH in case the MH is *normal* and δ_{CP} is close to $-\pi/2$, and more than 2σ C.L. sensitivity to CPV.

3.1.3 JUNO

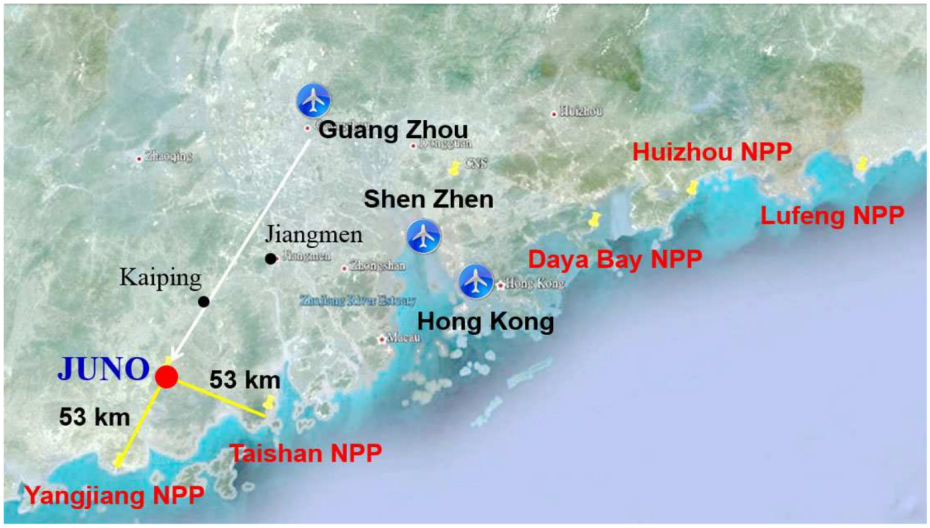

Figure 3-5: Location of JUNO site [22].

Jiangmen Underground Neutrino Observatory (JUNO) [22] is a reactor-based medium-baseline neutrino experiment, based in China. It is located in Jinji town, Kaiping city, Jiangmen city, Guangdong province. The geographic location is 112°31′05” longitude east and 22°07′05” latitude north, as shown in Figure 3-5. JUNO has an average baseline of 52.5 km and houses a 20 kton large liquid scintillator detector for detecting the electron anti-neutrinos ($\overline{\nu}_e$) from the Yangjiang (YJ) and Taishan (TS) nuclear power plants (NPPs) with an average baseline of 52.5 km. In JUNO, the electron antineutrino $\bar{\nu}_e$ flux comes mainly from four radioactive isotopes [23] ^{235}U, ^{238}U, ^{239}Pu, and ^{241}Pu, located at the reactor cores with an assumed detection efficiency of 73%. Each of the six cores at YJ nuclear plant will produce a power of 2.9 GW and the four cores at TS NPP will generate 4.6 GW each. They are combined to give 36 GW thermal power.

Table 3.1: Summary of the thermal power and baseline to the JUNO detector for the Yangjiang (YJ) reactor cores .

Cores	YJ-C1	YJ-C2	YJ-C3	YJ-C4	YJ-C5	YJ-C6
Power (GW)	2.9	2.9	2.9	2.9	2.9	2.9
Baseline (km)	52.75	52.84	52.42	52.51	52.12	52.21

Table 3.2: Summary of the thermal power and baseline to the JUNO detector for the Taishan (TS) reactor cores.

Cores	TS-C1	TS-C2	TS-C3	TS-C4
Power (GW)	4.6	4.6	4.6	4.6
Baseline (km)	52.76	52.63	52.32	52.20

The thermal power of all cores and the baselines are listed in Table 3.1 and 3.2.

3.1.3.1 JUNO Detector

The JUNO detector [22] consists of a central detector, a water Cherenkov detector and a muon tracker. The central detector is a liquid scintillator (LS) detector of 20 kton fiducial mass with an designed energy resolution of 3%/ E(MeV). The central detector is submerged in a water pool to be shielded from natural radioactivity from the surrounding rock and air. The water pool is equipped with Photomultiplier Tubes (PMTs) to detect the Cherenkov light from cosmic muons, acting as a veto detector. On top of the water pool, there is another muon detector to accurately measure the muon tracks. A schematic view of the JUNO detector is shown in Figure 3-6.

To realize practically the capability of mass hierarchy resolution, JUNO must achieve a very good neutrino energy resolution, which has been demonstrated recently in Ref. [24], and collect a huge amount of data. With six years of operation, JUNO can reach 3σ C.L. or higher sensitivity to the MH and achieve better than 1% precision on the solar neutrino parameters and the atmospheric neutrino mass-squared splitting $|\Delta m^2_{31}|$.

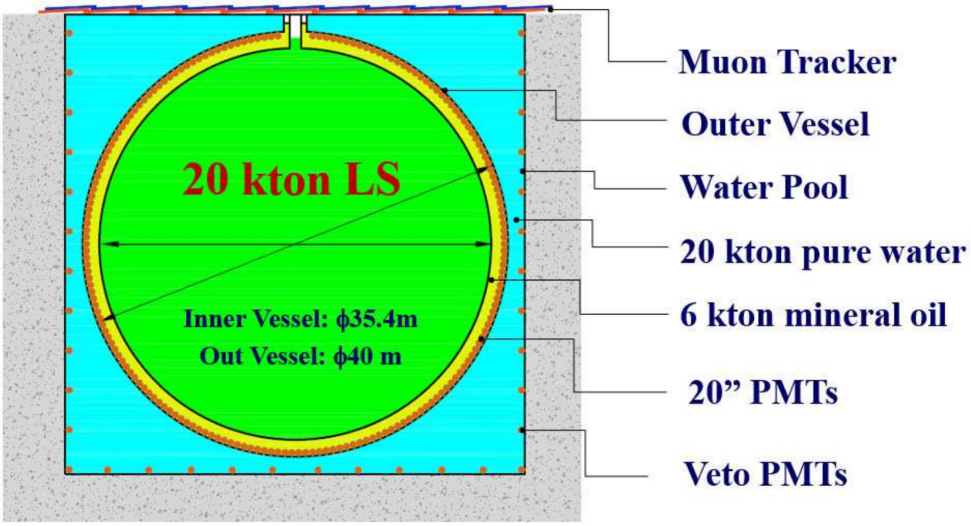

Figure 3-6: A schematic view of the JUNO detector [22] .

3.2 Simulation Technique

Although T2K and NOνA experiments have already collected with 18% and 36% of the total proton exposure assumed in this study, respectively, we do not directly use their experimental data to estimate their final reaches. The main reason is that measurements of the CP violation, the mass hierarchy, and the mixing angle θ_{23}, so far been statistically limited, except for a specific set of oscillation parameters. We thus carry out the study with the assumption that all values of $\delta_{\rm CP}$ and two scenarios of the neutrino mass hierarchy are still possible, and mixing angle θ_{23} is explored in a range close to 45°.

Reaching the three above mentioned *unknowns* depends on the ability to resolve the parameter degeneracies among $\delta_{\rm CP}$, the sign of Δm^2_{31}, θ_{13}, and θ_{23} [25]. Combining the data samples of the A-LBL experiments (T2K-II and NOνA-II) and JUNO would enhance the CPV search and MH determination since the JUNO sensitivity to MH has no ambiguity to $\delta_{\rm CP}$. To further enhance the CPV search, one can break the $\delta_{\rm CP}$-θ_{13} degeneracy by using the constraint of θ_{13} from reactor-based short-baseline (R-SBL) neutrino experiments such as Daya Bay [26], Double Chooz [27], and RENO [28]. This combination also helps to solve the θ_{23} octant in cases of non-maximal mixing.

3.2.1 GLoBES package

The General Long Baseline Experiment Simulator (GLoBES) [29, 30] is used for simulating the experiments and calculating the statistical significance. GLoBES is a software package to simulate A-LBL and reactor-based neutrino experiments. It is unable to describe solar and atmospheric neutrino experiments because in these experiments, one cannot assume the production of neutrinos to be stationary point sources. Within GLoBES, we define the experiments in a comprehensive Abstract Experiment Definition Language (AEDL). The AEDL file contains the externally feeded neutrino/antineutrino flux information and cross-section files of relevant neutrino interactions, run-time in neutrino/antineutrino mode, proton beam power, baseline, matter density profile, energy resolution functions, constant and variable energy bin widths, oscillation channels and energy-dependent detection efficiencies for a particular experiment that we want to simulate. For the systematics, energy normalization and calibration errors can be simulated in a straightforward way. It is then loaded in the user interface which is a C-library. Using GLoBES, we can compute the neutrino oscillation probabilities and the signal and background event rates. It allows to extract information in the level of event spectra and calculate the corresponding χ^2 values for different oscillation channels of an experiment or a combination of upto 32 experiments.

In this simulator, number of expected events of ν_j from ν_i oscillation in the n-th energy bin of the detector in a given experiment is calculated as

$$R_n(\nu_i \to \nu_j) = \frac{N}{L^2} \int_{E_n - \frac{\Delta E_n}{2}}^{E_n + \frac{\Delta E_n}{2}} dE_r \times \int dE_t \Phi_i(E_t) \sigma_{\nu_j} R_j(E_t, E_r) \epsilon_j(E_r) P_{\nu_i \to \nu_j}(E_t) \quad (3.1)$$

where,

- i, j are the charged lepton(s) associated with the initial and final flavor(s) of the neutrinos,
- Φ_i is the flux of the initial flavor at the source,
- σ_{ν_j} is the cross-section for the final flavor f,

- L is the baseline length,
- E_t and E_r are the incident and reconstructed neutrino energy, respectively,
- $\epsilon_j(E_r)$ is the detection efficiency of final flavor f, and
- N is the normalization factor for standard units in GLoBES.

$R_j(E_t, E_r)$ in the energy resolution function *i.e.* the probability to observe a reconstructed neutrino energy E_r, if the true neutrino energy is E_t. We consider a gaussian, given by

$$R_j(E_t, E_r) = \frac{1}{\sqrt{2\pi\sigma^2(E)}} e^{-\frac{(E_t - E_r)^2}{2\sigma^2(E)}} \tag{3.2}$$

with mean E_r and standard deviation $\sigma(E)$. We define the energy resolution function as follow:
For A-LBL,

$$\sigma(E) = p.E + q.\sqrt{E} + r \tag{3.3}$$

For R-MBL (relevant for inverse beta decay process),

$$\sigma(E) = \begin{pmatrix} p.\sqrt{1000}^{-1}\sqrt{(x-8).10^{-4}}, & \text{for } x > 1.8 \times 10^{-3} \\ p.10^{-3}, & \text{for } x \leq 1.8 \times 10^{-3} \end{pmatrix} \tag{3.4}$$

where the parameters p, q and r are provided by the user. For T2K-II, input parameters are $p = 0$, $q = 3\%$ and $= 8.5\%$ for both ν_μ ($\bar{\nu}_\mu$) and ν_e ($\bar{\nu}_e$) event reconstruction. For NOνA, the the definition of energy resolution function varies for different events which are given in Table 3.4. For JUNO, we define $p = 3\%$.

The latest results from the T2K and NOνA experiments on $\nu_\mu \to \nu_e$ ($\bar{\nu}_\mu \to \bar{\nu}_e$) appearances and $\nu_\mu \to \nu_\mu$ ($\bar{\nu}_\mu \to \bar{\nu}_\mu$) disappearance are given in Figure 3-7 and 3-8. The event spectra presented here for T2K are for Runs 1-9, from June, 2010 to May, 2018. That corresponds to an exposure of 14.94×10^{20} protons-on-target (POT) in ν-mode and 16.35×10^{20} POT in $\bar{\nu}$-mode. For NOνA, data taken in neutrino mode beam exposure of 13.6×10^{20} POT for a period from February, 2014 to March, 2020 and in antineutrino mode from June 29, 2016 to

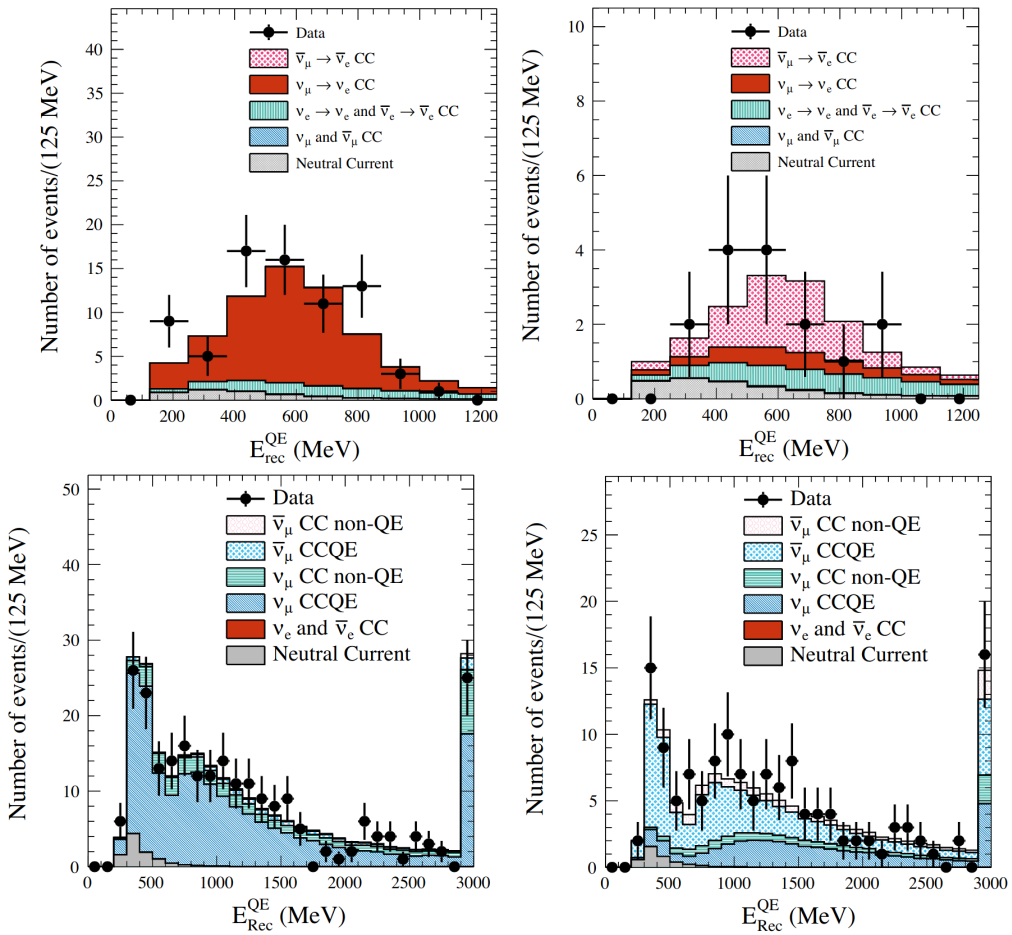

Figure 3-7: Recent results of T2K experiment. The *top* figures show the reconstructed energy distribution for ν_e appearance and the *bottom* figures represent the ν_μ disappearance events. The left (right) plot shows the events in neutrino (antineutrino) mode [31] .

February 26, 2019 is taken with an exposure of 12.5×10^{20} POT. During these periods, the proton beam was operated with an average power of 650 kW, with a peak at 756kW.

3.2.2 Neutrino Flux for T2K-II and NOνA-II

The flux predictions for the T2K SK far detector are provided in Figure 3-9. The original description of the flux predictions is published in [33]. Since the publication, the flux prediction has been updated with new thin target data from the NA61/SHINE experiment, and flux predictions for antineutrino enhanced beam operation have been produced. The NA61/SHINE thin target measurements of $\pi^\pm, K^\pm, K^0_S, \Lambda$ and p production are published in [34]. The updated flux

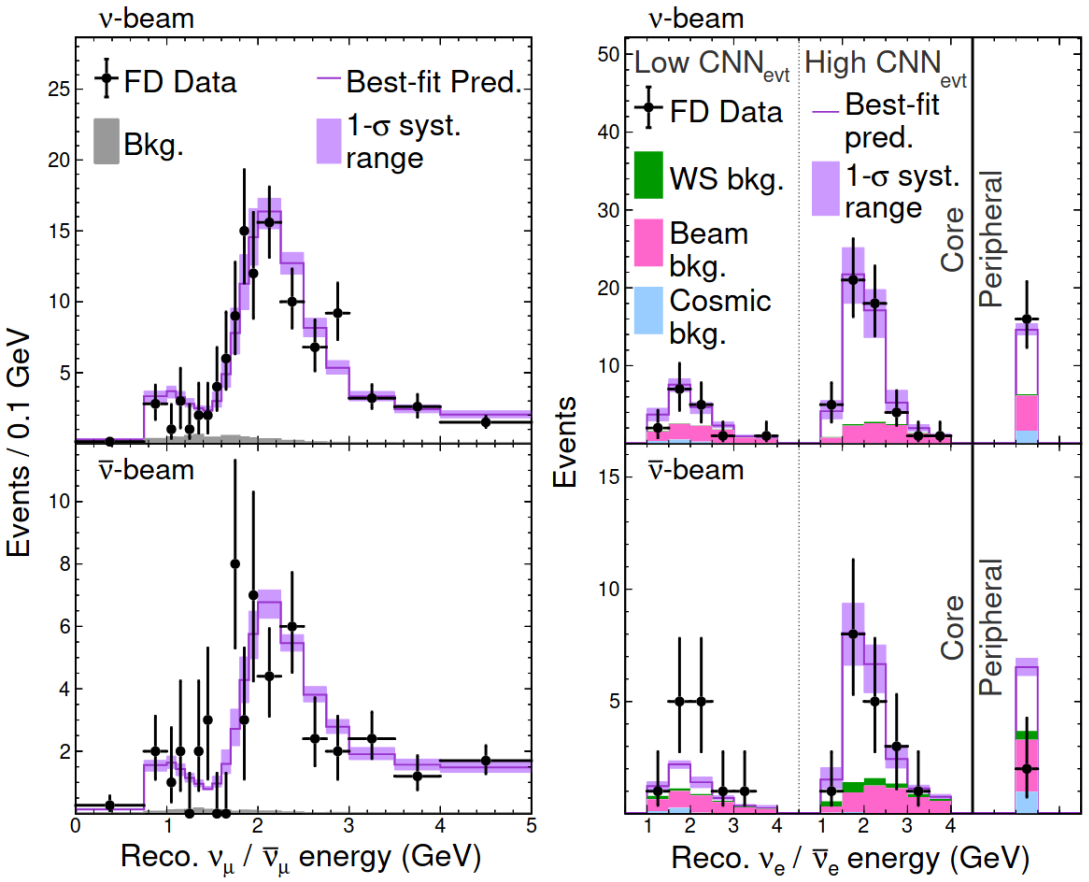

Figure 3-8: Reconstructed neutrino energy spectra for the NOνA FD. The *left* figures show the reconstructed energy distribution for $\nu_m u$ disappearance and the *right* figures represent the ν_e appearance events. The top (bottom) plot shows the events in neutrino (antineutrino) mode. The appearance events are classified in three bins from lowest to highest purity: "Peripheral", "Low PID", and "High PID" [32] .

prediction is described in [35]. The provided flux predictions include no neutrino oscillations. The SK flux is calculated for an infinitesimal angular range in a direction that is offset by 2.506° from the beam direction. The SK flux is calculated at a distance of 295.3 km from the center of the production target. Fluxes are provided for both +250 kA (neutrino enhanced beam) and -250 kA (antineutrino enhanced beam) operation of the T2K magnetic horns. The flux is given in 50 MeV wide bins of neutrino energy from 0 to 10 GeV neutrino energy. Above 10 GeV, the bins are 1 GeV wide, and are normalized to show the flux per 50 MeV. All flux predictions are normalized to 10^{21} protons delivered to the T2K production target. Figure 3-9 shows the flux distribution for the energy range 1-10 GeV in both neutrino and antineutrino modes.

For NOνA-II, we use the event spectra of [36] to construct the simulated experiment. The Monte Carlo information is available for 8.85×10^{20} POTs and 12.33×10^{20} POTs for neutrino and anti-neutrino respectively. We downloaded the ND flux files from the NOνA webpage [37] and reproduced as in Figure 3-10. The units of the files are in neutrinos/m^2/GeV/1M POT per year. We obtained the Far Detector fluxes corresponding to 10^{20} POT per year by scaling the ND fluxes with a factor of $1e14 \times \left[\frac{\text{ND baseline}}{\text{FD baseline}}\right]^2 = 1e14 \times (\frac{1km}{810km})^2$. The flux distribution for the FD is shown in Figure 3-11.

We describe the experiments using updated information of fluxes, signal and background efficiencies, and systematic errors. Remaining differences between the energy spectra of the simulated data sample at the reconstruction level obtained by GLoBES and the real experiment simulation can be due to the effects of the neutrino interaction model, the detector acceptance, detection efficiency variation as a function of energy, etc.. These differences are then treated quantitatively using post-smearing efficiencies, consequently allowing us to match our simulation with the published spectra of each simulated sample from each experiment.

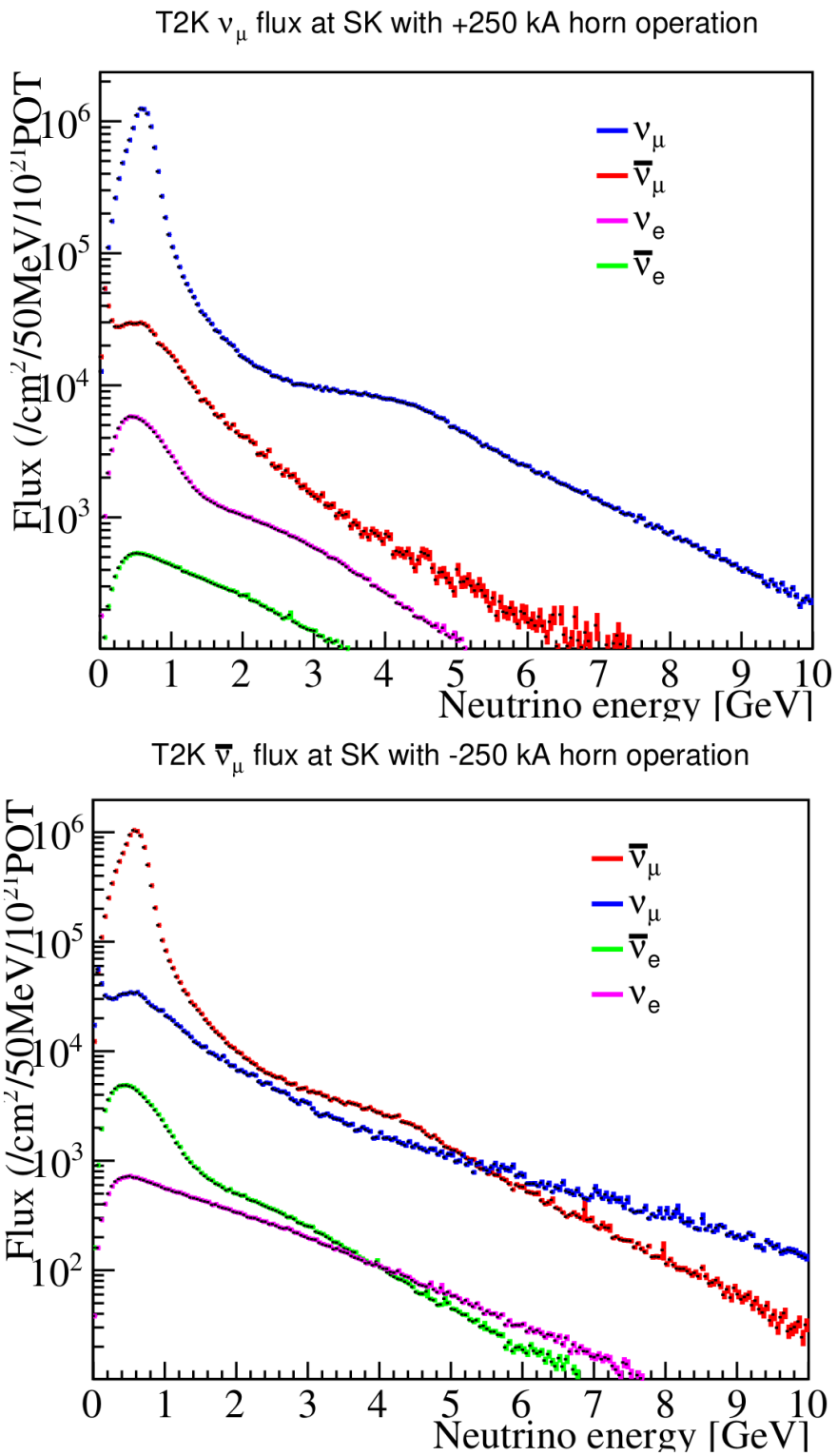

Figure 3-9: T2K flux at far detector for antineutrino mode (left pannel) and neutrino mode (right pannel), updated in 2016.

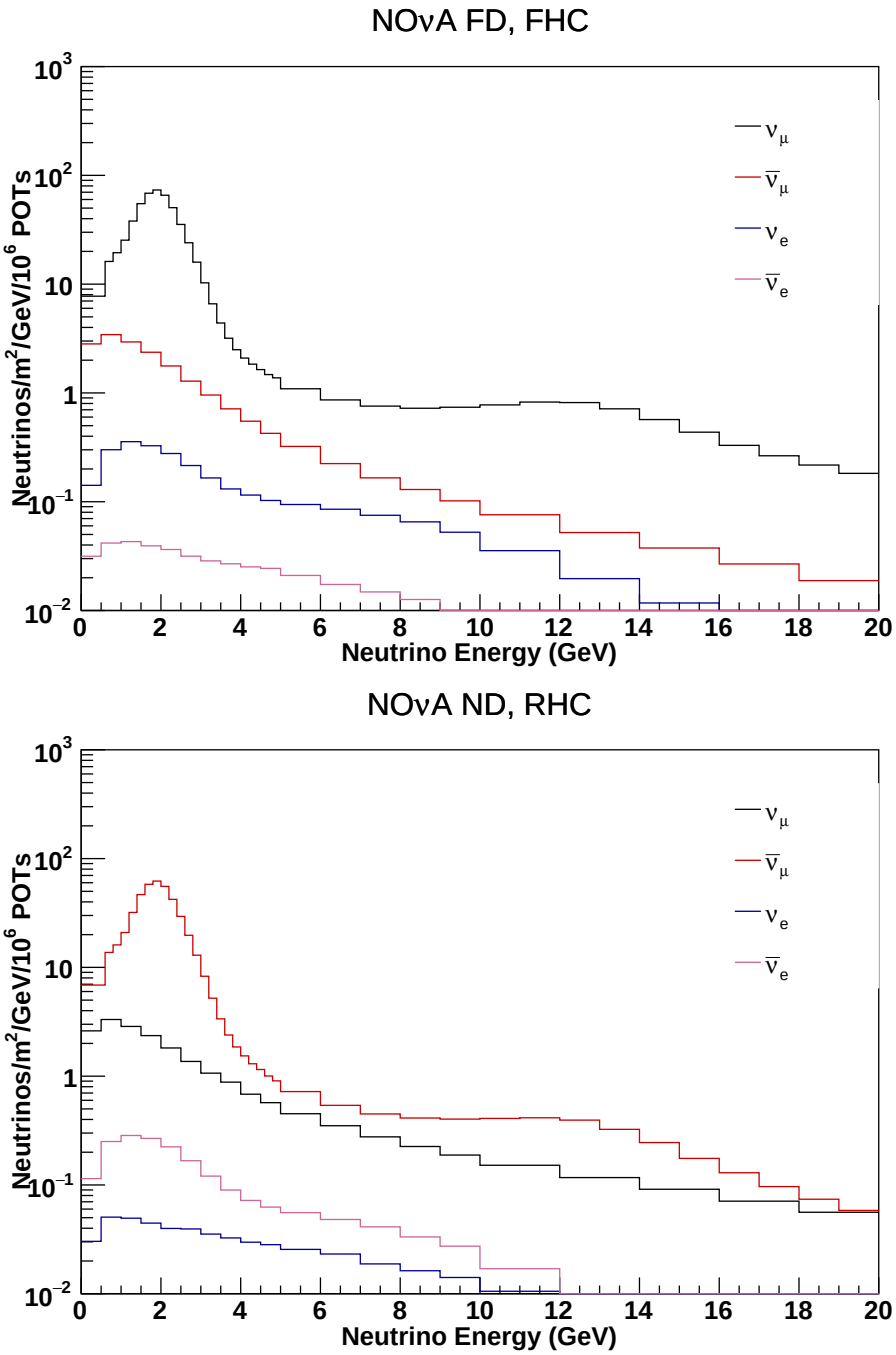

Figure 3-10: NOνA Near Detector Flux.

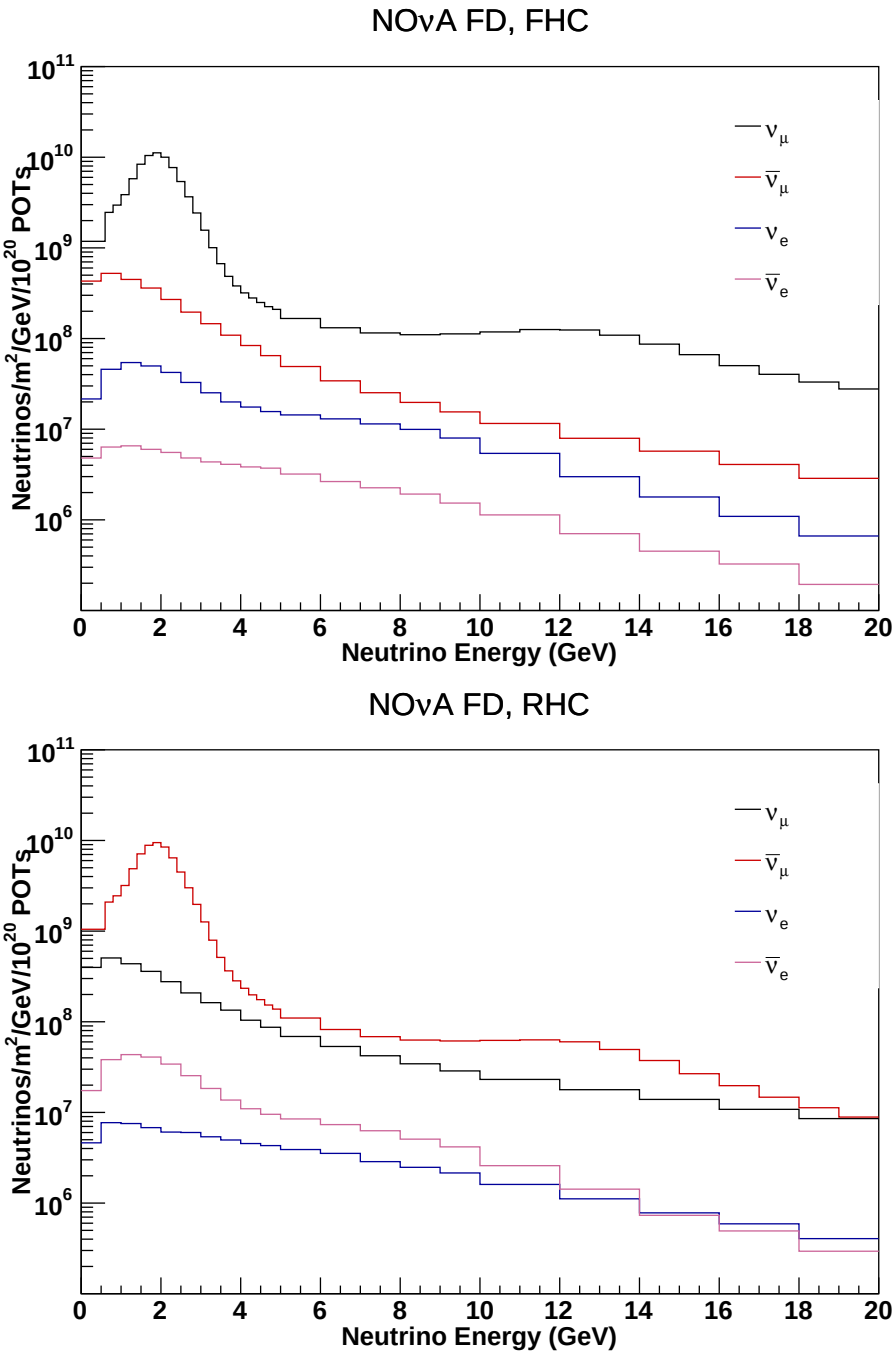

Figure 3-11: NOνA Far Detector Flux normalized to 10^{20} POTs per year.

3.3 Event Spectra

Each experimental setup is validated at the event rate level and sensitivity level to ensure that physics reaches of the simulated data samples we obtain are in relatively good agreement with the real experimental setup.

3.3.1 T2K-II and NOνA

For each of T2K-II and NOνA-II, four simulated data samples per each experiment are used: $\nu_\mu(\bar{\nu}_\mu)$ disappearance and $\nu_e(\bar{\nu}_e)$ appearance in both ν-mode and $\bar{\nu}$-mode. The experimental specifications of these two experiments are shown in Tables 3.3 and 3.4.

In T2K(-II), neutrino events are dominated by the Charged Current Quasi-Elastic (CCQE) interactions. Thus, for appearance (disappearance) in ν-mode and $\bar{\nu}$-mode, the signal events are obtained from the $\nu_\mu \to \nu_e$ ($\nu_\mu \to \nu_\mu$) CCQE events and $\bar{\nu}_\mu \to \bar{\nu}_e$ ($\bar{\nu}_\mu \to \bar{\nu}_\mu$) CCQE events, respectively.

Table 3.3: Experimental specifications of the A-LBL experiment T2K-II.

Characteristics	**T2K-II**[2, 38]
Baseline	295 km
Matter density [39]	2.6 gcc^{-1}
Total Exposure	20×10^{21} POT
Detector fiducial mass	22.5 kton
Systematics[1]	3% (0.01%)
Energy resolution	$0.03 \times \sqrt{\text{E(GeV)}}$
Energy window	0.1-1.3 GeV (APP[2]), 0.2-5.05 GeV (DIS[3])
Bin Width	0.125 GeV/bin (APP), 0.1 GeV/bin (DIS)

[1]normalization (calibration) error for both signals and backgrounds.

[2]shortened for the appearance sample.

[3]shortened for the disappearance sample.

Table 3.4: Experimental specifications of the A-LBL experiment NOνA-II.

Characteristics	**NOνA-II** [19, 21]
Baseline	810 km
Matter density	2.84 gcc^{-1}
Total Exposure	72×10^{20} POT
Detector fiducial mass	14 kton
Systematics	5% (2.5%)
Energy resolution	$x \times \sqrt{\text{E(GeV)}}$[1]
Energy window	0.0-4.0 GeV (*APP*), 0.0-5.0 GeV (*DIS*)
Bin Width	0.5 GeV/bin (*APP*), variable[2] (*DIS*)

[1] $x = 0.107$, 0.091, 0.088 and 0.081 for ν_e, ν_μ, $\bar{\nu}_e$ and $\bar{\nu}_\mu$ respectively.

[2] used the binning as in[19].

In the appearance samples, the intrinsic $\nu_e/\bar{\nu}_e$ contamination from the beam, the *wrong-sign* components i.e $\overline{\nu}_\mu \rightarrow \overline{\nu}_e$ ($\nu_\mu \rightarrow \nu_e$) in ν-mode ($\bar{\nu}$-mode) respectively, and the neutral current (NC) events constitute the backgrounds.

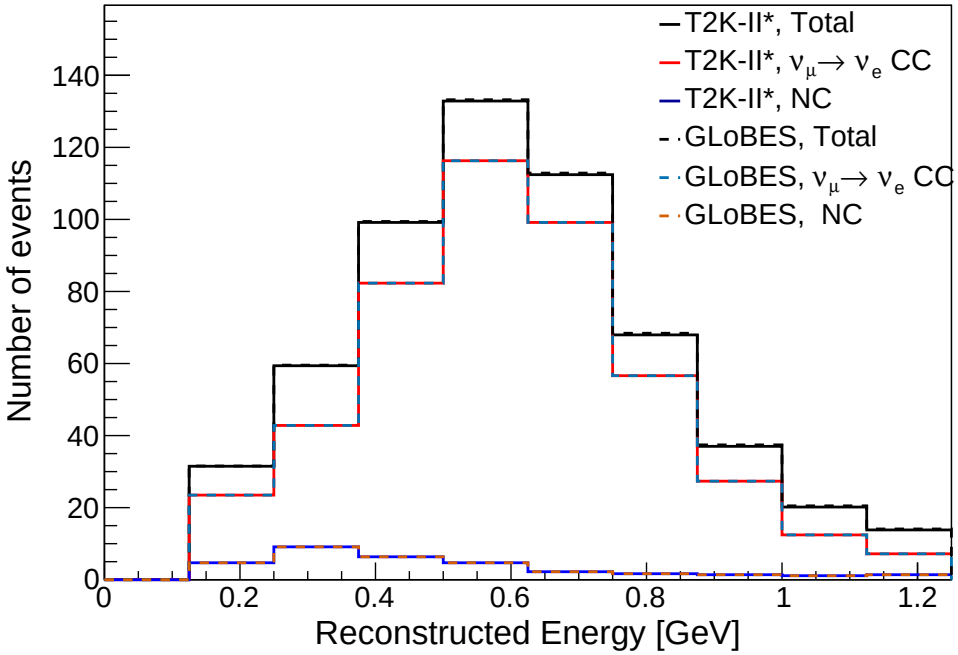

Figure 3-12: Expected event spectra of the signal and background as a function of reconstructed neutrino energy for T2K-II for appearance sample. The spectra are for ν-mode. Same oscillation parameters as Ref. [38] are used.

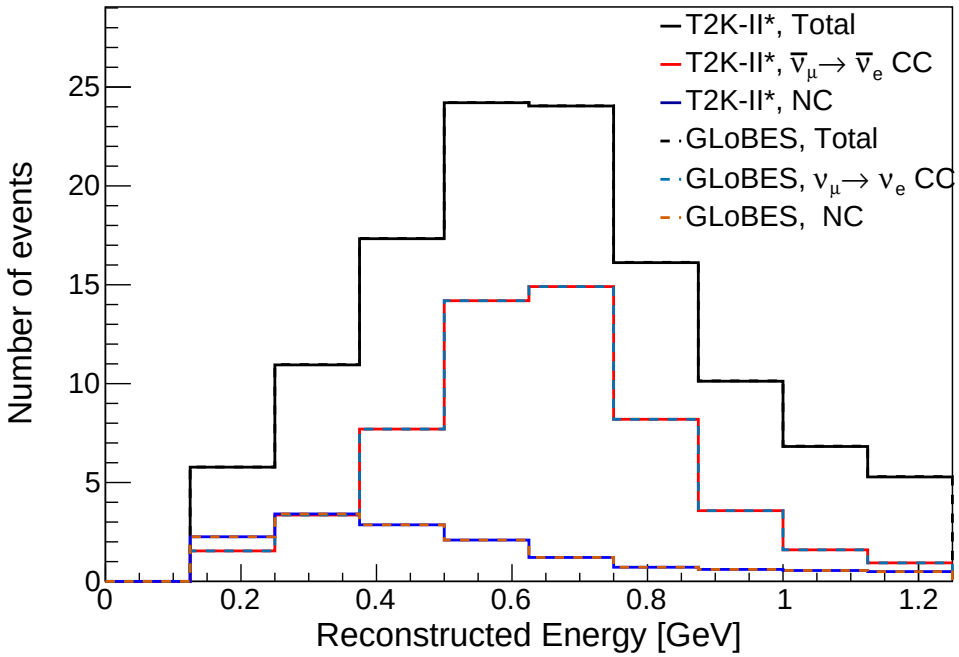

Figure 3-13: Same as Figure 3-12, but for $\bar{\nu}$-mode.

In the disappearance samples, the backgrounds come from ν_μ, $\overline{\nu}_\mu$ CC interaction excluding CCQE, hereby called CC-nonQE, and NC interactions. We use the updated T2K flux released along with Ref. [35]. In simulation, the cross section for low and high energy regions are taken from Ref. [40] and Ref. [41] respectively. In our T2K-II set-up, an exposure of 20×10^{21} POT equally divided among the ν-mode and the $\bar{\nu}$-mode is considered along with a 50% effectively statistic improvement as presented in Ref. [2]. The signal and background efficiencies and the spectral information for T2K-II are obtained by scaling the T2K analysis reported in Ref. [38] to same exposure as the T2K-II proposal. In Fig. 3-12 and 3-13, the T2K-II expected spectra of the signal and background events of

Table 3.5: Detection efficiencies(%)[a] of signal and background events in appearance samples. Normal mass hierarchy and $\delta_{CP} = 0$ are assumed.

		$\nu_\mu \rightarrow \nu_e$	$\bar{\nu}_\mu \rightarrow \bar{\nu}_e$	ν_μ CC	$\bar{\nu}_\mu$ CC	ν_e CC	$\bar{\nu}_e$ CC	NC
T2K-II	ν mode	65.5	46.2	0.02	0.02	19.8	19.8	0.41
	$\bar{\nu}$ mode	45.8	70.7	0.01	0.01	17.5	17.5	0.45
NOνA-II	ν mode	62.0	38.0	0.15	–	79.0	69.0	0.87
	$\bar{\nu}$ mode	25.0	67.0	0.14	0.05	20.7	40.7	0.51

[a]defined per each interaction channel as the ratio of selected events in the data sample to the totally simulated interaction supposed to happen in the detector.

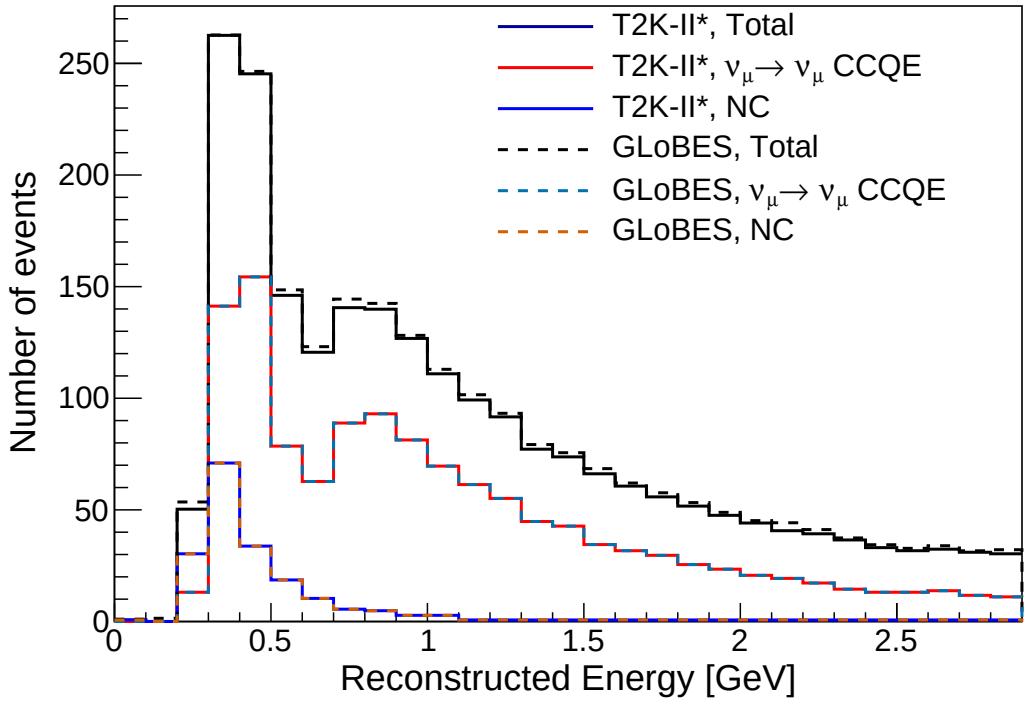

Figure 3-14: Expected event spectra of the signal and background as a function of reconstructed neutrino energy for T2K-II disappearance sample. The spectra are for ν-mode. Same oscillation parameters as Ref. [38] are used.

appearance samples as a function of reconstructed neutrino and antineutrino energy, respectively obtained with GLoBES are compared to those of Monte-Carlo simulation scaled from Ref. [2]. A 3% error is assigned for both the energy resolution and the normalization uncertainties of the signal and background in all simulated samples. Fig. 3-14 and 3-15 show the T2K-II expected spectra of the signal and background events of disappearance samples as a function of reconstructed neutrino energy.

For NOνA-II, we consider a total exposure of 72×10^{20} POT equally divided among ν-mode and $\bar{\nu}$-mode [21]. We predict the neutrino fluxes at the NOνA far detector by using the flux information from the near detector given in Ref. [37] and

Table 3.6: Detection efficiencies(%) of signal and background events in disappearance samples. Normal mass hierarchy is assumed .

		ν_μ CCQE	ν_μ CC non-QE	$\bar{\nu}_\mu$ CCQE	$\bar{\nu}_\mu$ CC non-QE	$(\nu_e + \bar{\nu}_e)$ CC	NC	$\nu_\mu \to \nu_e$
T2K-II	ν mode	71.2	20.4	71.8	20.4	0.84	2.7	0.84
	$\bar{\nu}$ mode	65.8	24.5	77.5	24.5	0.58	2.5	0.58
NOνA-II	ν mode	31.2[b]		27.2		–	0.44	–
	$\bar{\nu}$ mode	33.9		20.5		–	0.33	–

[b]the efficiencies for CCQE and CC non-QE interactions are considered equal.

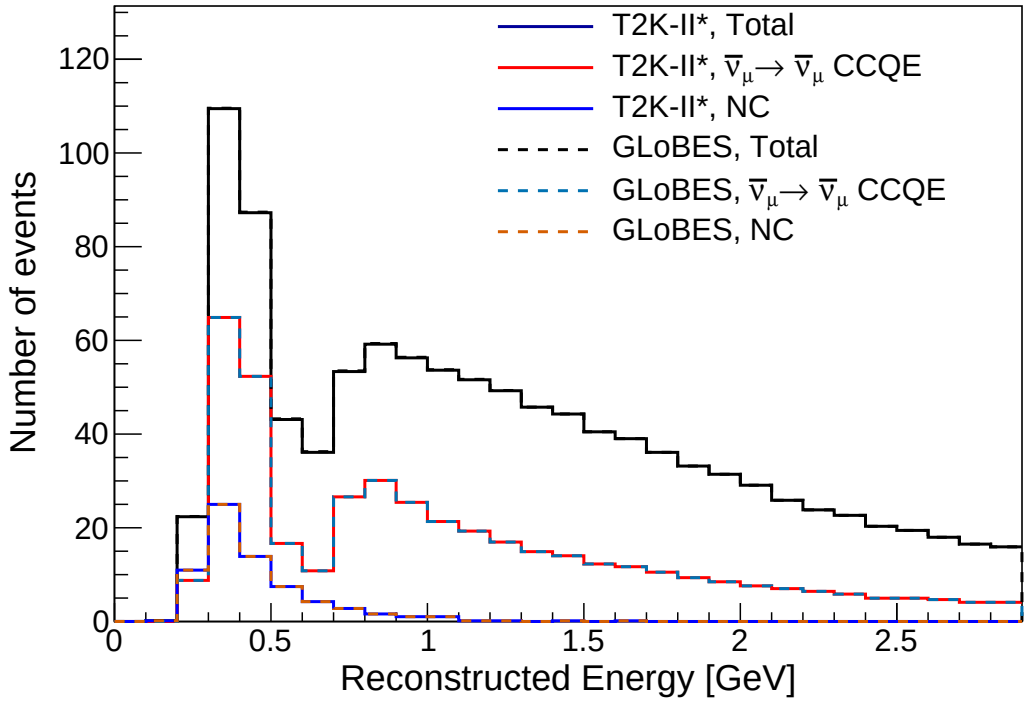

Figure 3-15: Same as Figure 3-14, but for $\bar{\nu}$-mode.

normalizing it with the square of their baseline ratio. A 5% systematic error for all samples and 8-10% sample-dependent energy resolutions are assigned. Significant background events in the appearance samples stem from the intrinsic beam $\nu_e/\bar{\nu}_e$, NC components, and cosmic muons. In the appearance sample of the $\bar{\nu}$-mode, *wrong-sign* events from ν_e appearance events are included as the backgrounds in the simulation. We use the reconstructed energy spectra of the NOνA far detector simulated sample reported in Ref. [42] to tune our GLoBES simulation. The low- and high-particle identification (PID) score samples are used but not the peripheral sample since the reconstructed energy information is not available. In the disappearance samples of both ν-mode and $\bar{\nu}$-mode, events from both CC ν_μ and $\bar{\nu}_\mu$ interactions are considered as signal events, which is tuned to match with the NOνA far detector simulated signal given an identical exposure. Background from the NC ν_μ ($\bar{\nu}_\mu$) interactions is taken into consideration and weighted such that the rate at a predefined exposure is matched to a combination of the reported NC and cosmic muon backgrounds in Ref. [42]. Fig. 3-16 and 3-17 show the simulated NOνA-II event spectra for ν_e appearance as a function of reconstructed neutrino energy, in both ν-mode and $\bar{\nu}$-mode, where *normal* MH is assumed, $\delta_{\rm CP}$

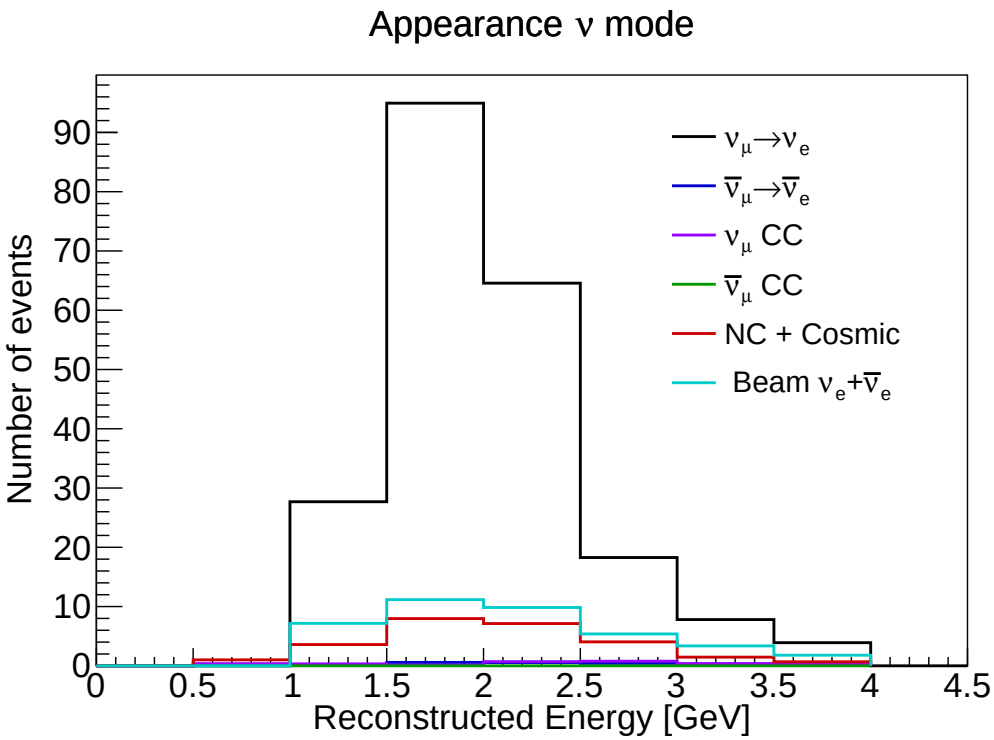

Figure 3-16: Expected event spectra of the signal and background as a function of reconstructed neutrino energy for NOνA-II for the appearance channel. The spectra are for ν-mode. *Normal* MH, $\delta_{\text{CP}} = 0$, and other oscillation parameters given in Tab. 2.1 are assumed.

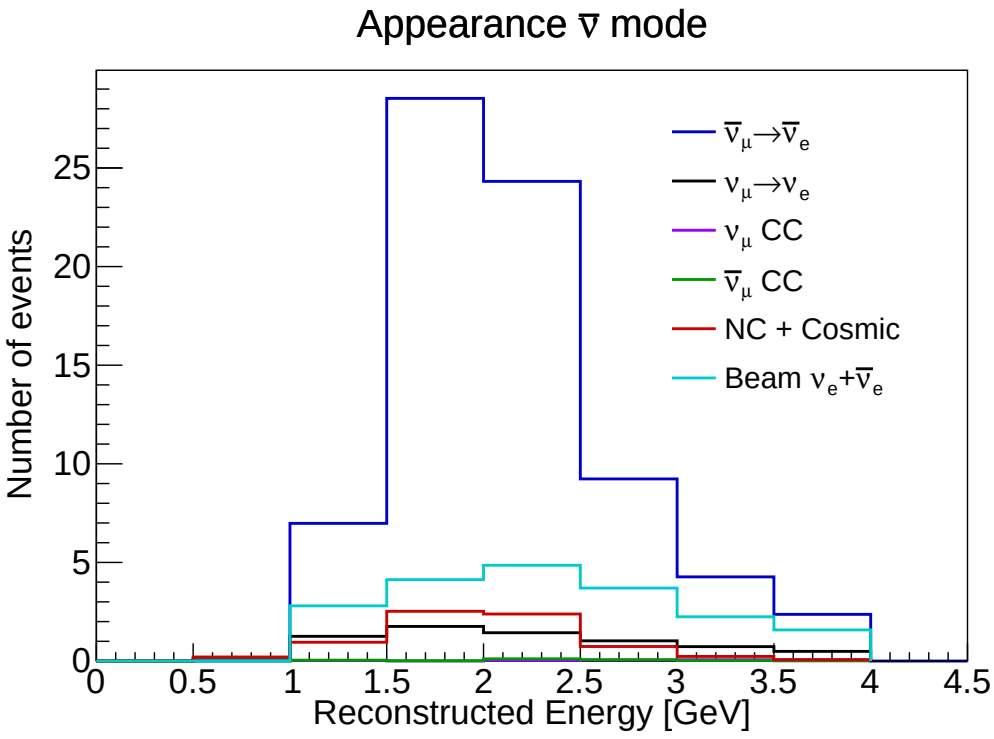

Figure 3-17: Same as Figure 3-16, but for $\bar{\nu}$-mode.

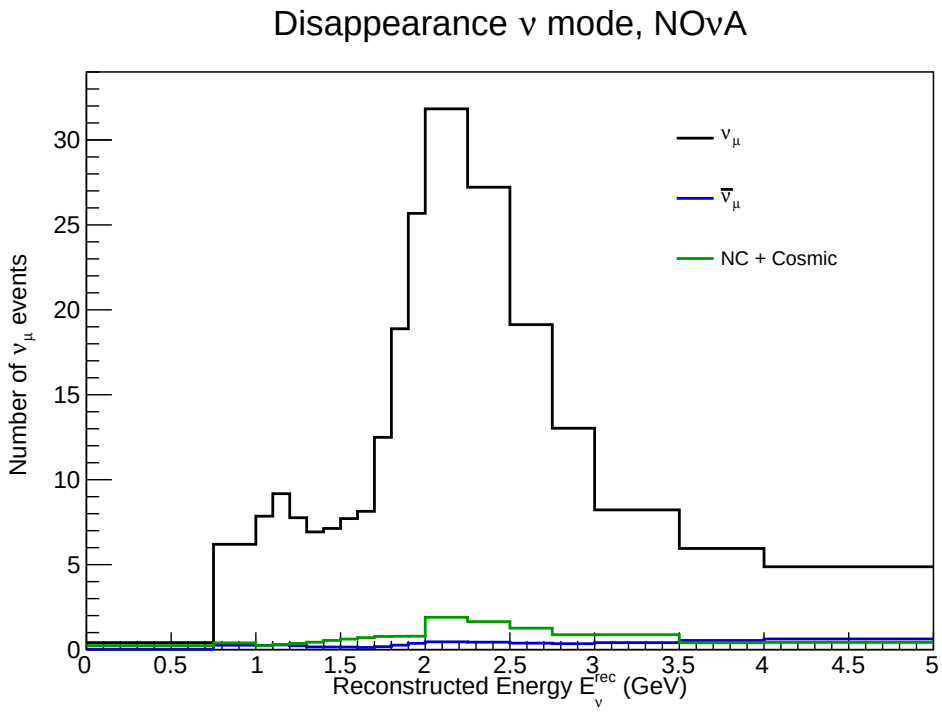

Figure 3-18: Expected event spectra of the signal and background as a function of reconstructed neutrino energy for NOνA-II for disappearance channel. The spectra are for ν-mode. *Normal* MH, $\delta_{\text{CP}} = 0$, and other oscillation parameters given in Tab. 2.1 are assumed.

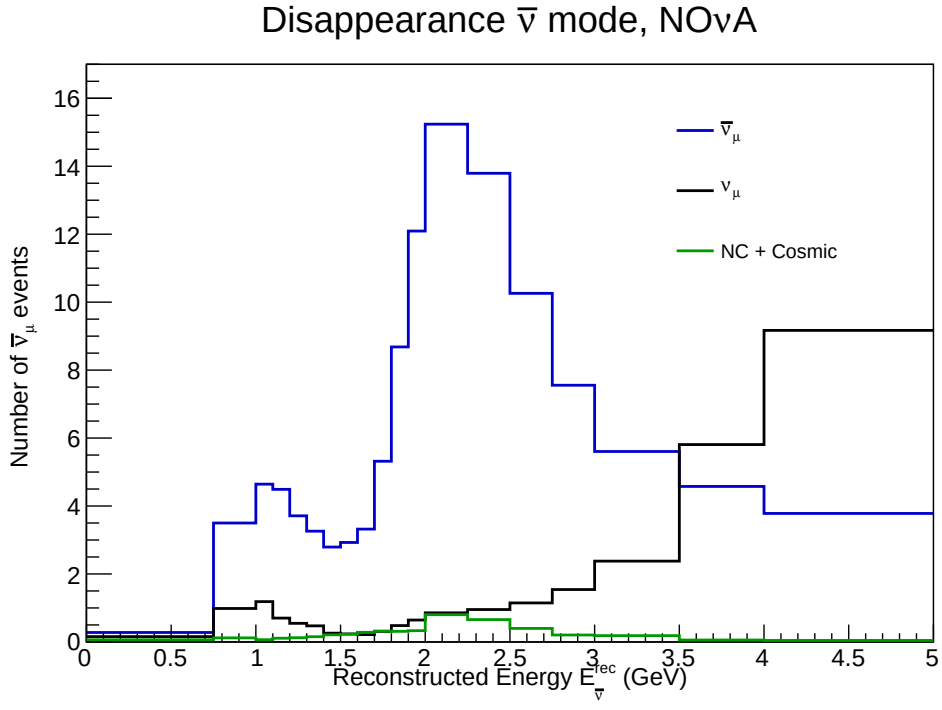

Figure 3-19: Same as Figure 3-18, but for $\bar{\nu}$-mode.

is fixed at 0°, and other parameters are given in Table 2.1. The event spectra for ν_μ disappearance channels in neutrino and antineutrino mode are presented in Figures 3-18 and 3-19, respectively. Tables 3.5 and Table 3.6 detail our calculated signal and background detection efficiencies for the electron (anti-)neutrino appearance and muon (anti-)neutrino disappearance respectively in T2K and NOνA.

3.3.2 JUNO

In JUNO, the electron anti-neutrino $\bar{\nu}_e$ flux, which is produced mainly from four radioactive isotopes ^{235}U, ^{238}U, ^{239}Pu, and ^{241}Pu [23], is simulated with an assumed detection efficiency of 73%. The backgrounds, which have a marginal effect on the MH sensitivity, are not included in our simulation. In our setup, to speed up the calculation, we consider one core of 36 GW thermal power with an average baseline of 52.5 km instead of the true distribution of the reactor cores, baselines, and powers. The simulated JUNO specification is listed in Table 3.7.

For systematic errors, we use 1% commonly for the errors associated with the uncertainties of the normalization of the $\bar{\nu}_e$ flux produced from the reactor core, the normalization of the detector mass, the spectral normalization of the signal, the detector response to the energy scale, the isotopic abundance, and the bin-to-bin reconstructed energy shape.

Table 3.7: JUNO simulated specifications

Characteristics	Inputs
Baseline	52.5 km
Density	2.8 gcc^{-1} [43]
Detector type	Liquid Scintillator
Detector mass	20 kton
$\bar{\nu}_e$ Detection Efficiency	73%
Running time	6 years
Thermal power	36 GW
Energy resolution	$3\% \ / \sqrt{\text{E (MeV)}}$
Energy window	1.8-9 MeV
Number of bins	200

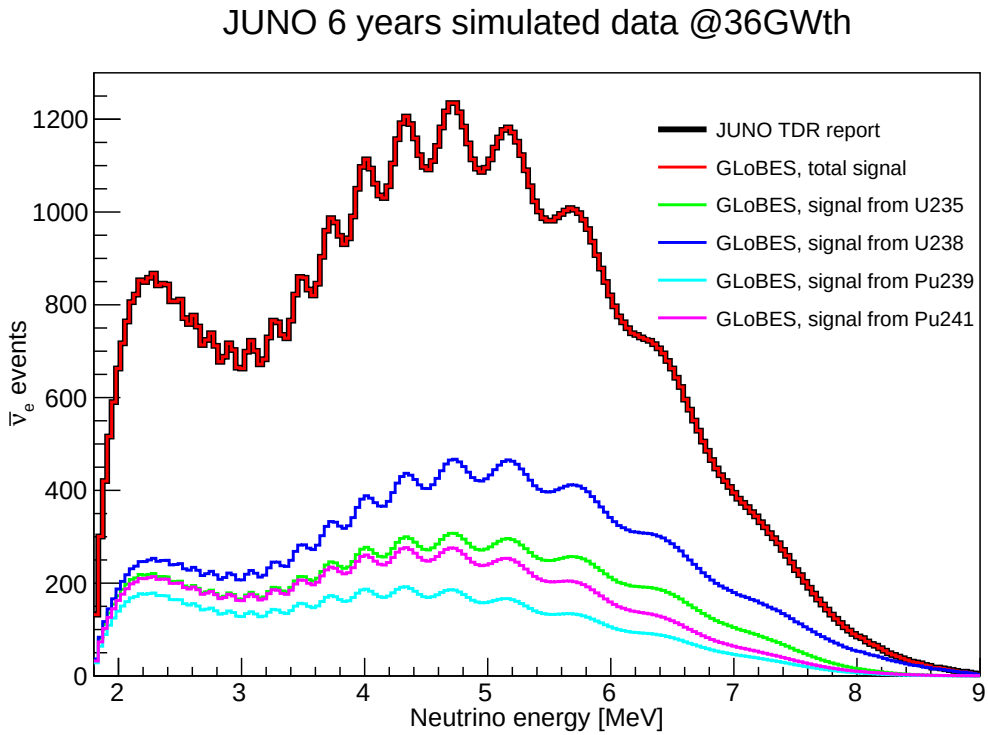

Figure 3-20: JUNO event rate calculated at same oscillation parameters as Ref. [22]

3.4 Discussion

The two neutrino experiments T2K-II and NOνA-II reach a relatively similar performance for selecting the electron (anti-)neutrino appearance samples. While T2K-II gains to the excellent separation of muons and electrons with the water Cherenkov detector, NOνA-II boosts the selection performance with the striking features of the liquid scintillator and the powerful deep learning. For selecting the disappearance samples, T2K outperforms since the T2K far detector is placed deep underground while the NOvA far detector is on the surface and suffers a much higher rate of cosmic ray muons. Besides T2K-II, NOνA-II, and JUNO, we implement a R-SBL neutrino experiment to constrain $\sin^2\theta_{13}$ at 3% uncertainty, which is reachable as prospected in Ref. [44]. This constraint is important to break the parameter degeneracy between δ_{CP}-θ_{13}, which is inherent from the measurement with the electron (anti-)neutrino appearance samples in the A-LBL experiments.

Bibliography

[1] **T2K Collaboration** *et al.* The T2K experiment. *Nuclear Instruments and Methods in Physics Research Section A: Accelerators, Spectrometers, Detectors and Associated Equipment* **659**, 106–135, 2011. 1106.1238.

[2] **T2K Collaboration** *et al.* Sensitivity of the T2K accelerator-based neutrino experiment with an extended run to 20×10^{21} POTs , 2016. 1607.08004.

[3] **Hyper-Kamiokande Proto-Collaboration** *et al.* Hyper-Kamiokande Design Report , 2018. 1805.04163.

[4] Otani, M. *et al.* Design and construction of INGRID neutrino beam monitor for T2K neutrino experiment. *Nucl. Instrum. Meth. A* **623**, 368–370, 2010.

[5] Abgrall, N. *et al.* Time Projection Chambers for the T2K Near Detectors. *Nucl. Instrum. Meth. A* **637**, 25–46, 2011. 1012.0865.

[6] Amaudruz, P. A. *et al.* The T2K Fine-Grained Detectors. *Nucl. Instrum. Meth. A* **696**, 1–31, 2012. 1204.3666.

[7] Abe, K. *et al.* Measurements of the T2K neutrino beam properties using the INGRID on-axis near detector. *Nucl. Instrum. Meth. A* **694**, 211–223, 2012. 1111.3119.

[8] Itow, Y. *et al.* The JHF-Kamioka neutrino project. In *3rd Workshop on Neutrino Oscillations and Their Origin (NOON 2001)*. 239–248, 2001. hep-ex/0106019.

[9] Fukuda, Y. *et al.* Measurements of the solar neutrino flux from super-kamiokande's first 300 days. *Physical review letters* **81** (6), 1158, 1998.

[10] Abe, K. *et al.* The T2K experiment. *Nuclear Instruments and Methods in Physics Research Section A: Accelerators, Spectrometers, Detectors and Associated Equipment* **659** (1), 106–135, 2011.

[11] Fukuda, Y. *et al.* The Super-Kamiokande detector. *Nucl. Instrum. Meth. A* **501**, 418–462, 2003.

[12] **T2K Collaboration** *et al.* Observation of electron neutrino appearance in a muon neutrino beam. *Physical Review Letters* **112**, 061802, 2014. 1311.4750.

[13] **T2K Collaboration** *et al.* Constraint on the matter-antimatter symmetry-violating phase in neutrino oscillations. *Nature* **580** (7803), 339–344, 2020. [Erratum: Nature 583, E16 (2020)], 1910.03887.

[14] Dunne, P. Latest neutrino oscillation results from T2K, 2020. URL https://doi.org/10.5281/zenodo.4154355.

[15] **NOνA Collaboration** *et al.* The NOvA Technical Design Report , 2007.

[16] Kafka, T. MINOS Experiment at Fermilab. *Prog. Part. Nucl. Phys.* **64**, 184–186, 2010.

[17] Adamson, P. *et al.* The NuMI Neutrino Beam. *Nucl. Instrum. Meth. A* **806**, 279–306, 2016. 1507.06690.

[18] Nayak, N. *A Joint Measurement of ν_μ-Disappearance and ν_e-Appearance in the NuMI beam using the NOvA Experiment*. Ph.D. thesis, UC, Irvine (main), UC, Irvine, 2021.

[19] **NOνA Collaboration** *et al.* First measurement of neutrino oscillation parameters using neutrinos and anti-neutrinos by NOνA. *Physical Review Letters* **123** (15), 151803, 2019. 1906.04907.

[20] Himmel, A. New oscillation results from the nova experiment, 2020. URL https://doi.org/10.5281/zenodo.4142045.

[21] **NOνA Collaboration,** M. Sanchez. NOνA results and prospects. *XXVIII International Conference on Neutrino Physics and Astrophysics* , 2018.

[22] **JUNO Collaboration** *et al.* JUNO Conceptual Design Report , 2015. 1508.07166.

[23] Huber, P. & Schwetz, T. Precision spectroscopy with reactor anti-neutrinos. *Physical Review D* **70** (5), 053011, 2004. 0407026.

[24] Abusleme, A. *et al.* Calibration Strategy of the JUNO Experiment , 2020. 2011.06405.

[25] Barger, V. *et al.* Breaking eight fold degeneracies in neutrino CP violation, mixing, and mass hierarchy. *Phys. Rev. D* **65**, 073023, 2002. hep-ph/0112119.

[26] **Daya Bay Collaboration** *et al.* A Precision measurement of the neutrino mixing angle θ_{13} using reactor antineutrinos at Daya-Bay , 2007. 0701029.

[27] **Double Chooz Collaboration** *et al.* Double Chooz: A Search for the neutrino mixing angle theta(13) , 2006. 0606025.

[28] **RENO Collaboration** *et al.* RENO: An Experiment for Neutrino Oscillation Parameter θ_{13} Using Reactor Neutrinos at Yonggwang , 2010. 1003.1391.

[29] Huber, P. *et al.* Simulation of long-baseline neutrino oscillation experiments with GLoBES (General Long Baseline Experiment Simulator). *Computer Physics Communications* **167**, 195, 2005. 0407333.

[30] Huber, P. *et al.* New features in the simulation of neutrino oscillation experiments with GLoBES 3.0. *Computer Physics Communications* **177** (5), 432–438, 2007. hep-ph/0701187.

[31] Abe, K. *et al.* Improved constraints on neutrino mixing from the T2K experiment with $\mathbf{3.13 \times 10^{21}}$ protons on target. *Phys. Rev. D* **103** (11), 112008, 2021. 2101.03779.

[32] Acero, M. A. *et al.* An Improved Measurement of Neutrino Oscillation Parameters by the NOvA Experiment , 2021. 2108.08219.

[33] Abe, K. *et al.* T2K neutrino flux prediction. *Phys. Rev. D* **87** (1), 012001, 2013. [Addendum: Phys.Rev.D 87, 019902 (2013)], 1211.0469.

[34] Abgrall, N. *et al.* Measurements of $\pi^{\pm}$, $K^{\pm}$, K^0_S , Λ and proton production in proton–carbon interactions at 31 GeV/c with the NA61/SHINE spectrometer at the CERN SPS. *Eur. Phys. J. C* **76** (2), 84, 2016. 1510.02703.

[35] Abe, K. *et al.* Measurements of neutrino oscillation in appearance and disappearance channels by the T2K experiment with 6.6×10^{20} protons on target. *Phys. Rev. D* **91** (7), 072010, 2015. 1502.01550.

[36] **NOνA Collaboration,** A. Himmel. New Oscillation Results from the NOνA Experiment. In *XXIX International Conference on Neutrino Physics and Astrophysics*, 2020.

[37] Soplin, L. A. & Cremonesi, L. NOνA near detector fluxes. https://nova-docdb.fnal.gov/cgi-bin/ShowDocument?docid=25266, 2018.

[38] **T2K Collaboration** *et al.* Measurement of neutrino and antineutrino oscillations by the T2K experiment including a new additional sample of ν_e interactions at the far detector. *Physical Review D* **96** (9), 092006, 2017. [Erratum: Phys.Rev.D 98, 019902 (2018)], 1707.01048.

[39] Dziewonski, A. M. & Anderson, D. L. Preliminary reference earth model (PREM). *Physics of the earth and planetary interiors* **25** (4), 297–356, 1981.

[40] Messier, M. D. *Evidence for neutrino mass from observations of atmospheric neutrinos with Super-Kamiokande*. Ph.D. thesis, Boston University, 1999. UMI-99-23965.

[41] Paschos, E. A. & Yu, J. Y. Neutrino interactions in oscillation experiments. *Physical Review D* **65**, 033002, 2002. hep-ph/0107261.

[42] **NOνA Collaboration** *et al.* New constraints on oscillation parameters from ν_e appearance and ν_μ disappearance in the NOνA experiment. *Physical Review D* **98** (3), 032012, 2018. 1806.00096.

[43] Khan, A. N. *et al.* Why matter effects matter for JUNO? *Physics Letters B* **803**, 135354, 2020. 1910.12900.

[44] Cao, J. & Luk, K.-B. An overview of the Daya Bay Reactor Neutrino Experiment. *Nucl. Phys. B* **908**, 62–73, 2016. 1605.01502.